Resource

Cell

Programmable RNA Tracking in Live Cells with CRISPR/Cas9

Graphical Abstract

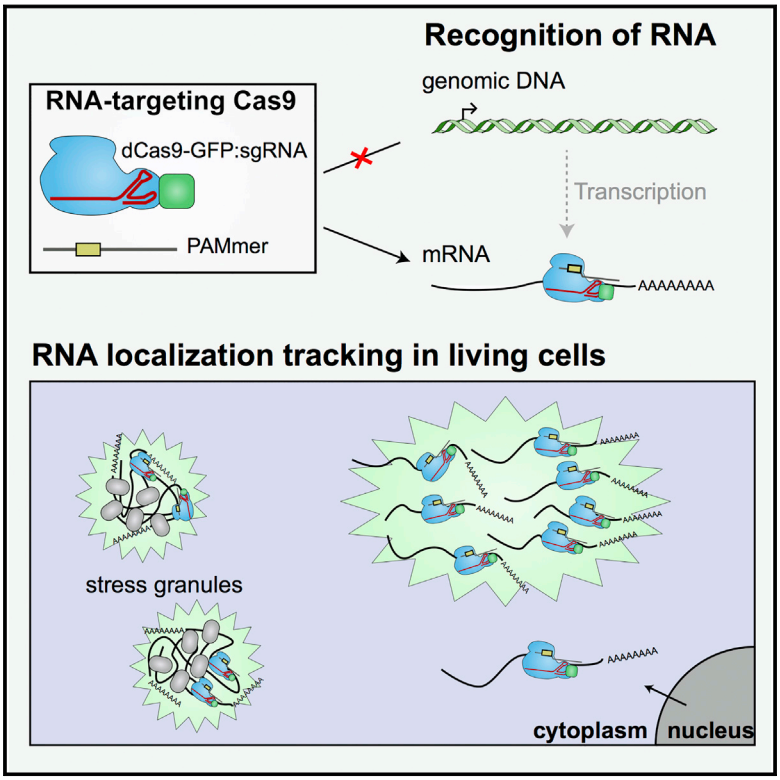

Highlights

- RNA-targeting Cas9 (RCas9) enabled recognition of endogenous, unmodified mRNAs
- RCas9 did not influence mRNA abundance or amount of translated protein
- Subcellular distribution of RCas9 was highly correlated with RNA-FISH
- RCas9 revealed trafficking of mRNAs to stress granules in live cells

Authors

David A. Nelles, Mark Y. Fang, Mitchell R. O'Connell, Jia L. Xu, Sebastian J. Markmiller, Jennifer A. Doudna, Gene W. Yeo

Correspondence

geneyeo@ucsd.edu

In Brief

RNA-targeting Cas9 enables tracking of endogenous, untagged mRNA, establishing CRISPR/Cas9 as a programmable system to recognize RNA in live cells.

Nelles et al., 2016, Cell *165*, 1–9
April 7, 2016 ©2016 Elsevier Inc.
http://dx.doi.org/10.1016/j.cell.2016.02.054

CellPress

Please cite this article in press as: Nelles et al., Programmable RNA Tracking in Live Cells with CRISPR/Cas9, Cell (2016), http://dx.doi.org/10.1016/j.cell.2016.02.054

Cell

Programmable RNA Tracking in Live Cells with CRISPR/Cas9

David A. Nelles,[1,2] Mark Y. Fang,[1] Mitchell R. O'Connell,[4] Jia L. Xu,[1] Sebastian J. Markmiller,[1] Jennifer A. Doudna,[4,5,6] and Gene W. Yeo[1,2,3,*]

[1]Department of Cellular and Molecular Medicine and Institute for Genomic Medicine, University of California, San Diego, La Jolla, CA 92037, USA

[2]Materials Science and Engineering Graduate Program, University of California, San Diego, La Jolla, CA 92093, USA

[3]Department of Physiology, Yong Loo Lin School of Medicine, National University of Singapore, Singapore 1190777, Singapore

[4]Department of Molecular and Cell Biology and Center for RNA Systems Biology, University of California, Berkeley, Berkeley, CA 94720, USA

[5]Department of Chemistry, Innovative Genomics Initiative and Howard Hughes Medical Institute, University of California, Berkeley, Berkeley, CA 94720, USA

[6]Physical Biosciences Division, Lawrence Berkeley National Laboratory, Berkeley, Berkeley, CA 94720, USA

*Correspondence: geneyeo@ucsd.edu

http://dx.doi.org/10.1016/j.cell.2016.02.054

SUMMARY

RNA-programmed genome editing using CRISPR/Cas9 from *Streptococcus pyogenes* has enabled rapid and accessible alteration of specific genomic loci in many organisms. A flexible means to target RNA would allow alteration and imaging of endogenous RNA transcripts analogous to CRISPR/Cas-based genomic tools, but most RNA targeting methods rely on incorporation of exogenous tags. Here, we demonstrate that nuclease-inactive *S. pyogenes* CRISPR/Cas9 can bind RNA in a nucleic-acid-programmed manner and allow endogenous RNA tracking in living cells. We show that nuclear-localized RNA-targeting Cas9 (RCas9) is exported to the cytoplasm only in the presence of sgRNAs targeting mRNA and observe accumulation of *ACTB*, *CCNA2*, and *TFRC* mRNAs in RNA granules that correlate with fluorescence in situ hybridization. We also demonstrate time-resolved measurements of *ACTB* mRNA trafficking to stress granules. Our results establish RCas9 as a means to track RNA in living cells in a programmable manner without genetically encoded tags.

INTRODUCTION

Clustered regularly-interspaced short palindromic repeats (CRISPRs) form the basis of adaptive immune systems in bacteria and archaea by encoding CRISPR RNAs that guide CRISPR-associated (Cas) nucleases to invading genetic material (Wiedenheft et al., 2012). Cas9 from the type II CRISPR system of *S. pyogenes* has been repurposed for genome engineering in eukaryotic organisms (Hwang et al., 2013; Li et al., 2013a; Mali et al., 2013; Nakayama et al., 2013; Sander and Joung, 2014; Yang et al., 2014) and is rapidly proving to be an efficient means of DNA targeting for other applications such as gene expression modulation (Qi et al., 2013) and imaging (Chen et al., 2013). Cas9 and its associated single-guide RNA (sgRNA) require two critical features to target DNA: a short DNA sequence of the form 5′-NGG-3′ (where "N" = any nucleotide) known as the protospacer adjacent motif (PAM) and an adjacent sequence on the opposite DNA strand that is antisense to the sgRNA. By supporting DNA recognition with specificity determined entirely by a short spacer sequence within the sgRNA, CRISPR/Cas9 provides uniquely flexible and accessible manipulation of the genome. Manipulating cellular RNA content, in contrast, remains problematic. Whereas there exist robust means of attenuating gene expression via RNAi and antisense oligonucleotides, other critical aspects of post-transcriptional gene expression regulation such as subcellular trafficking, alternative splicing or polyadenylation, and spatiotemporally restricted translation are difficult to measure in living cells and are largely intractable.

Analogous to the assembly of zinc finger nucleases (Urnov et al., 2010) and transcription activator-like effector nucleases (TALEN) to recognize specific DNA sequences, efforts to recognize specific RNA sequences have focused on engineered RNA-binding domains. Pumilio and FBF homology (PUF) proteins carry well-defined modules capable of recognizing a single base each and have supported successful targeting of a handful of transcripts for imaging and other manipulations (Filipovska et al., 2011; Ozawa et al., 2007; Wang et al., 2009). PUF proteins can be fused to arbitrary effector domains to alter or tag target RNAs, but PUFs must be redesigned and validated for each RNA target and can only recognize eight contiguous bases, which does not allow unique discrimination in the transcriptome. Molecular beacons are self-quenched synthetic oligonucleotides that fluoresce upon binding to target RNAs and allow RNA detection without construction of a target-specific protein (Sokol et al., 1998). But molecular beacons must be microinjected to avoid the generation of excessive background signal associated with endosome-trapped probes and are limited to imaging applications. An alternative approach to recognition of RNA substrates is to introduce RNA aptamers into target RNAs, enabling specific and strong association of cognate aptamer-binding proteins such as the MS2 coat protein (Fouts

et al., 1997). This approach has enabled tracking of RNA localization in living cells over time with high sensitivity (Bertrand et al., 1998) but relies upon laborious genetic manipulation of the target RNA and is not suitable for recognition of arbitrary RNA sequences. Furthermore, insertion of exogenous aptamer sequence has the potential to interfere with endogenous RNA functions. Analogous to CRISPR/Cas9-based recognition of DNA, programmable RNA recognition based on nucleic acid specificity alone without the need for genetic manipulation or libraries of RNA-binding proteins would greatly expand researchers' ability to modify the mammalian transcriptome and enable transcriptome engineering.

Although the CRISPR/Cas9 system has evolved to recognize double-stranded DNA, recent in vitro work has demonstrated that programmable targeting of RNAs with Cas9 is possible by providing the PAM as part of an oligonucleotide (PAMmer) that hybridizes to the target RNA (O'Connell et al., 2014). By taking advantage of the Cas9 target search mechanism that relies on PAM sequences (Sternberg et al., 2014), a mismatched PAM sequence in the PAMmer/RNA hybrid allows exclusive targeting of RNA and not the encoding DNA. The high affinity and specificity of RNA recognition by Cas9 in cell-free extracts and the success of genome targeting with Cas9 indicate the potential of CRISPR/Cas9 to support programmable RNA targeting in living cells.

To assess the potential of Cas9 as a programmable RNA-binding protein in live cells, we used a modified sgRNA scaffold with improved expression and Cas9 association (Chen et al., 2013) with a stabilized PAMmer oligonucleotide that does not form a substrate for RNase H. We measured the degree of nuclear export of a nuclear localization signal-tagged nuclease-deficient Cas9-GFP fusion and demonstrate that the sgRNA alone is sufficient to promote nuclear export of Cas9 without influencing the abundance of the targeted mRNA or encoded protein. In order to evaluate whether RNA-targeting Cas9 (RCas9) signal patterns correspond with an established untagged RNA-labeling method, we compared distributions of RCas9 and fluorescence in situ hybridization (FISH) targeting *ACTB* mRNA. We observed high correlation among FISH and RCas9 signal that was dependent on the presence of a PAMmer, indicating the importance of the PAM for efficient RNA targeting. RNA trafficking and subcellular localization are critical to gene expression regulation and reaction to stimuli such as cellular stress. To address whether RCas9 allows tracking of RNA to oxidative stress-induced RNA/protein accumulations called stress granules, we measured *ACTB*, *TFRC*, and *CCNA2* mRNA association with stress granules in cells subjected to sodium arsenite. Finally, we demonstrated the ability of RCas9 to track trafficking of *ACTB* mRNA to stress granules over time in living cells. This work establishes the ability of RCas9 to bind RNA in live cells and sets the foundation for manipulation of the transcriptome in addition to the genome by CRISPR/Cas9.

RESULTS

RNA-Targeting Cas9 Export from Nucleus in Presence of sgRNA Targeting GAPDH mRNA

We initially assessed the ability of RCas9 to recognize specific mRNA substrates in human cells by evaluating the degree of nuclear export of a nuclear-localized RCas9 system. Specifically, we tested whether mCherry-tagged Cas9 containing a nuclear localization signal (NLS) can be co-exported from the nucleus with an mRNA in the presence of a cognate sgRNA and PAMmer designed to recognize that mRNA (Figure 1A). Nuclease null Cas9 (dCas9) was fused to two SV40 NLS sequences at the C terminus with the coding sequence for mCherry and cloned into a mammalian expression vector (dCas9-2xNLS-mCherry, abbreviated as dCas9-mCherry). In a separate expression vector, a modified sgRNA scaffold with an extended stem-loop structure that improves association with Cas9 and mutations that eliminate a partial transcription termination sequence (Chen et al., 2013) was driven by the U6 small nuclear RNA (snRNA) polymerase III promoter. The PAMmer was synthesized as a mixed DNA and 2′-*O*-methyl (2′OMe) RNA oligonucleotide using standard phosphoramidite chemistry and purified using high-performance liquid chromatography (HPLC) (see Tables S1 and S2 for target mRNA, sgRNA, and PAMmer sequences). As a proof of concept, we designed a sgRNA-PAMmer pair to target the 3′ UTR of *GAPDH* mRNA (Figure 1B). As a negative control, we designed a sgRNA-PAMmer pair targeting a sequence in the λ bacteriophage that is absent in human cells ("N/A" sgRNA and PAMmer and "λ2" sgRNA and PAMmer sequences in Tables S1 and S2). We observed that transiently transfected dCas9-mCherry co-transfected with the negative control sgRNA and PAMmer is almost exclusively nuclear with only 12% of cells containing greater mCherry signal in the cytoplasm compared to the nucleus (Figures 1B and 1C). When the negative control PAMmer was replaced with the *GAPDH*-targeting PAMmer, the results were identical. Importantly, upon co-transfection of *GAPDH*-targeting sgRNA plasmid, we observed that 84% of cells had greater mCherry signal in the cytoplasm. Interestingly, even with a non-targeting PAMmer, 79% of cells had predominantly cytoplasmic mCherry signal, suggesting that the sgRNA is the primary determinant of RNA substrate recognition. Indeed, the sgRNA targeting *GAPDH* resulted in a significant increase in the fraction of cells with cytoplasmic mCherry signal compared to a non-targeting sgRNA (Figure 1C). Overall, these results are consistent with previous in vitro RNA pull-down experiments showing that RNA binding by Cas9:sgRNA is independent of but strengthened by the PAMmer (O'Connell et al., 2014). Thus, we demonstrate that RCas9 RNA recognition is programmable with a sgRNA and a PAMmer designed to target a specific, abundant mRNA in live cells.

Recognition of an mRNA with RNA-Targeting Cas9 Does Not Alter RNA Abundance or Amount of Translated Protein

To further characterize the interaction between RCas9 and a target mRNA, we directed RCas9 to the 3′ UTR of *Renilla* luciferase carrying a commonly used RNA tag for RNA tracking from the MS2 bacteriophage (Fouts et al., 1997) and a sequence targeted by a previously validated sgRNA:PAMmer pair ("λ2"; see Table S2; O'Connell et al., 2014; Figure 1D). RNA immunoprecipitation with an antibody recognizing EGFP revealed a 4-fold greater association of luciferase mRNA to dCas9-EGFP in the presence of a cognate sgRNA and PAMmer compared to non-targeting sgRNA (sense to the λ2 RNA sequence) with a

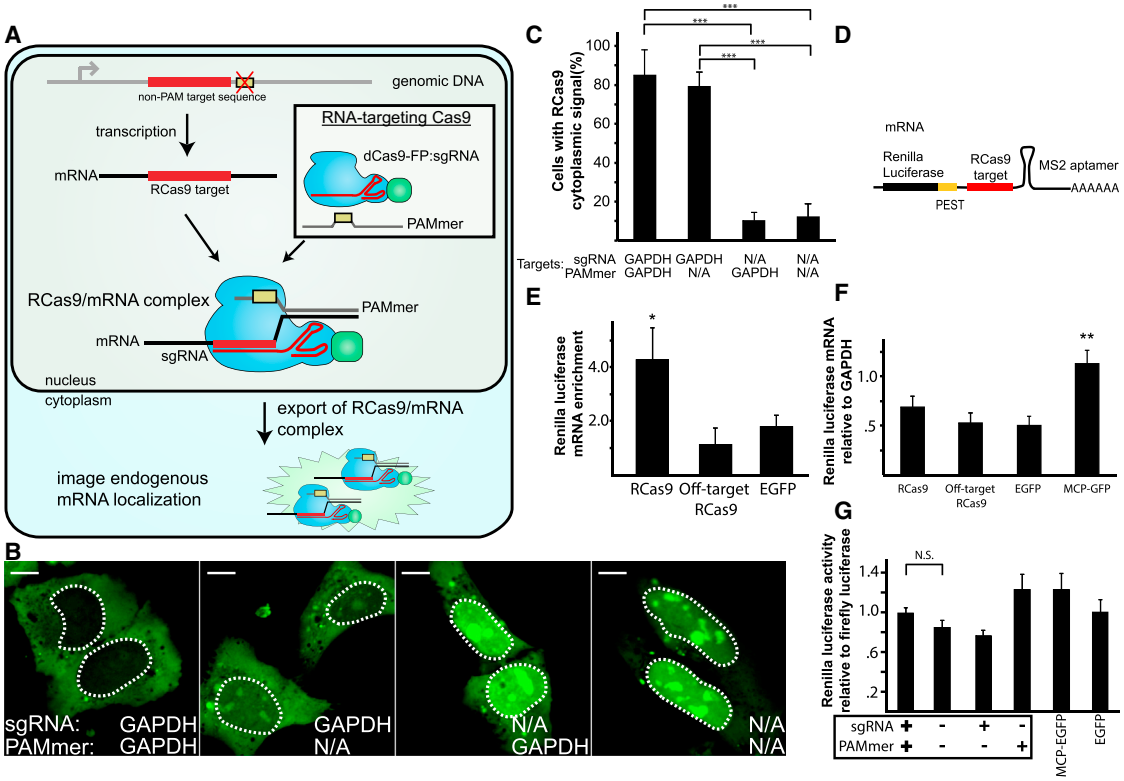

Figure 1. Targeting mRNA in Living Cells with RCas9

(A) Components required for RNA-targeting Cas9 (RCas9) recognition of mRNA include a nuclear localization signal-tagged nuclease-inactive Cas9 fused to a fluorescent protein such as GFP, a modified sgRNA with expression driven by the U6 polymerase III promoter, and a PAMmer composed of DNA and 2′-*O*-methyl RNA bases with a phosphodiester backbone. The sgRNA and PAMmer are antisense to adjacent regions of the target mRNA whose encoding DNA does not carry a PAM sequence. After formation of the RCas9/mRNA complex in the nucleus, the complex is exported to the cytoplasm.

(B) RCas9 nuclear co-export with *GAPDH* mRNA. The RCas9 system was delivered to U2OS cells with a sgRNA and PAMmer targeting the 3′ UTR of *GAPDH* or sgRNA and PAMmer targeting a sequence from λ bacteriophage that should not be present in human cells ("N/A"). Cellular nuclei are outlined with a dashed white line. Scale bars represent 5 microns.

(C) Fraction of cells with cytoplasmic RCas9 signal. Mean values ± SD (n = 50).

(D) A plasmid carrying the *Renilla* luciferase open reading frame with a β-globin 3′ UTR containing a target site for RCas9 and MS2 aptamer. A PEST protein degradation signal was appended to luciferase to reveal any translational effects of RCas9 binding to the mRNA.

(E) RNA immunoprecipitation of EGFP after transient transfection of the RCas9 system in HEK293T cells targeting the luciferase mRNA compared to non-targeting sgRNA and PAMmer or EGFP alone. Mean values ± SD (n = 3).

(F and G) *Renilla* luciferase mRNA (F) and protein (G) abundances were compared among the targeting and non-targeting conditions. Mean values ± SD (n = 4). p values are calculated by Student's t test, and one, two, and three asterisks represent p values less than 0.05, 0.01, and 0.001, respectively. See also Figure S1.

scrambled PAMmer or to EGFP protein alone (Figure 1E). We next measured the effect of RCas9 targeting on luciferase mRNA abundance by qRT-PCR. We observed no significant difference in the abundance of MS2-tagged luciferase mRNA in the presence of the targeting or non-targeting RCas9 system or EGFP alone. In contrast, co-expression of EGFP fused to the MS2 coat protein (MCP) recognizing the MS2 aptamer had a significant stabilizing effect (Figure 1F). We also considered potential effects of RCas9 targeting on translation of luciferase (Figure 1G) and observed that the presence of the targeting sgRNA and PAMmer caused no significant changes in protein levels compared to non-targeting RCas9. To confirm that the RCas9/sgRNA/PAMmer complex does not perturb its endogenous RNA substrates, we evaluated the influence of RCas9 targeting on *ACTB* and *GAPDH* mRNAs. We transiently transfected the RCas9 system and isolated transfected cells using fluorescence-activated cell sorting (FACS) gated on cells positive for both Cas9 and sgRNA transfection. We observed no significant differences in *GAPDH* and *ACTB* mRNA or protein levels as measured by western blot and qRT-PCR among samples with RCas9-targeting *ACTB* mRNA, *GAPDH* mRNA, cells transfected with GFP instead of dCas9-GFP, and RCas9-targeting sequence from λ bacteriophage (Figure S1; Tables S1 and S2). Our results demonstrate that RCas9 recognition of RNA with a sgRNA and PAMmer does not perturb RNA and encoded protein levels.

Correlation of RNA-Targeting Cas9 Signal Distributions with an Established Untagged RNA Localization Measurement

To assess whether RCas9 signal distributions correlate with an orthogonal method to measure RNA localization, we targeted the 3′ UTR of *ACTB* ("+" sgRNA and "+" PAMmer) and compared

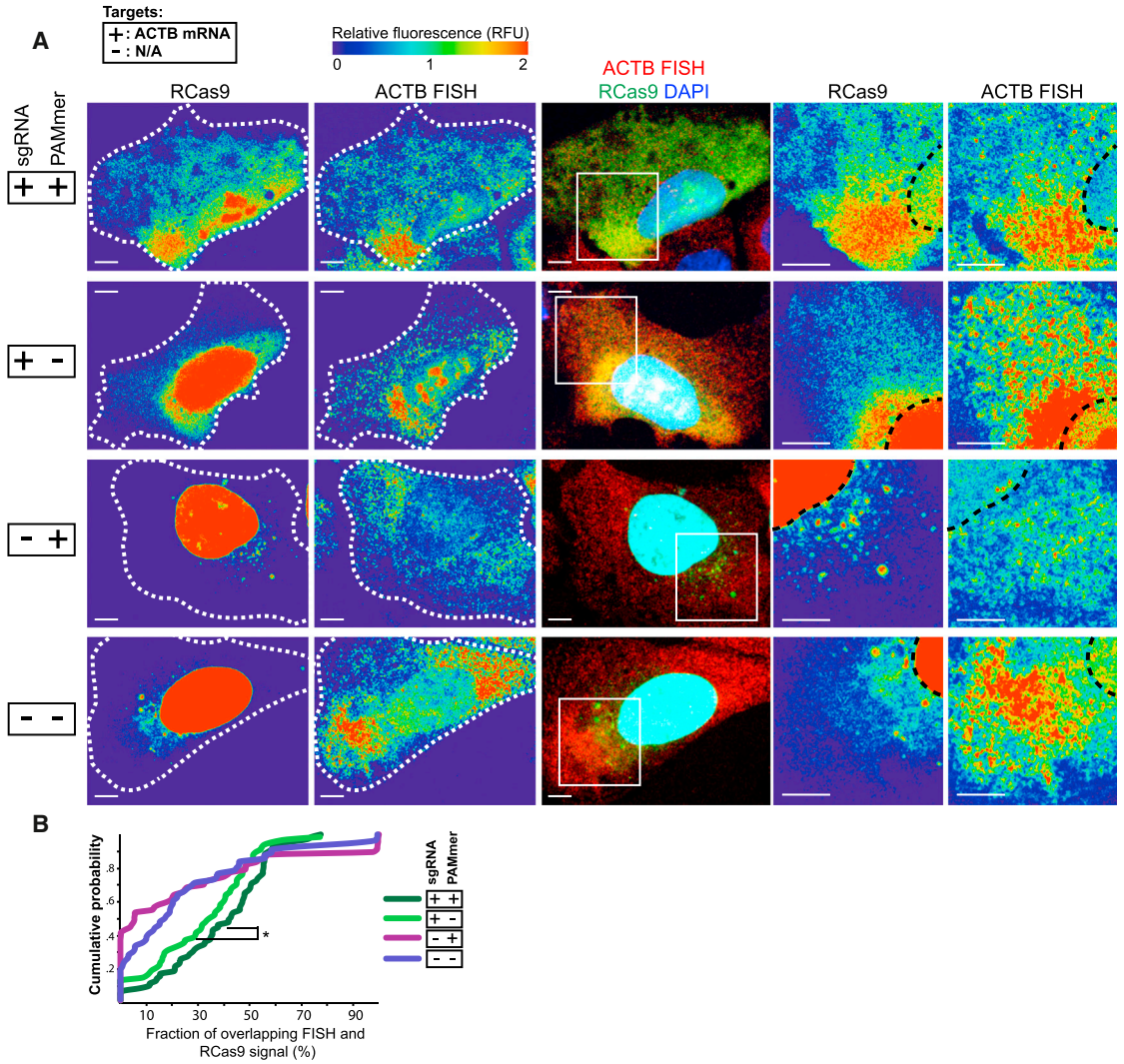

Figure 2. *ACTB* mRNA Localization with RCas9 Compared to FISH

(A) The RCas9 system was delivered to U2OS cells, and the cells were subjected to FISH for *ACTB* mRNA. RCas9 with sgRNA- and PAMmer-targeting *ACTB* mRNA was compared to non-targeting sgRNA and PAMmer antisense to a sequence from λ bacteriophage ("–" sgRNA and "–" PAMmer). White dotted lines delineate the cellular boundaries, and black dotted lines delineate cellular nuclei. Scale bars represent 5 microns. Insets (on right) are delineated by white boxes.

(B) Pixel-by-pixel analysis of RCas9 and FISH colocalization using the Manders' overlap coefficient is summarized with a cumulative distribution of the percent of cytoplasmic area with overlapping signal in 60–80 cells in each condition. The presence of the PAMmer produces a significantly greater colocalization among RCas9 and FISH in the presence of the sgRNA-targeting *ACTB* mRNA ($p = 0.035$; two-tailed Mann-Whitney U test).

See also Figure S2.

dCas9-GFP signal to RNA FISH for *ACTB* mRNA (Figure 2A) and non-targeting sgRNA and PAMmer ("–" sgRNA and "–" PAMmer with sequences corresponding to λ bacteriophage). By comparing the Manders' overlap coefficients that describe pixel-by-pixel overlap among FISH and RCas9 (Manders et al., 1992; Figures 2B and S2), we determined that the sgRNA primarily accounts for colocalization among FISH and RCas9 with maximal overlap in the presence of both sgRNA- and PAMmer-targeting *ACTB* mRNA. A non-targeting PAMmer results in significantly less overlap (Figure 2B; $p = 0.035$; Mann-Whitney U test) and produces a diffuse pattern of RCas9 signal in the cytoplasm that contrasts with the highly localized pattern revealed by FISH (Figure 2A). This result is consistent with weaker binding of RCas9 with a non-targeting PAMmer observed in cell-free systems (O'Connell et al., 2014). A non-targeting sgRNA results in largely nuclear retention of RCas9 signal with low correlation between cytoplasmic RCas9 signal and FISH (Figures 2A and 2B). We conclude that the localization patterns of single EGFP-fused RCas9 in live cells correlates surprisingly well with localization obtained by FISH using tens of probes per mRNA in fixed cells.

Tracking RNA Trafficking to Stress Granules over Time

Many polyadenylated RNAs including *ACTB* mRNA are known to localize to stress granules (Unsworth et al., 2010) during

oxidative stress. We simultaneously tracked *ACTB* mRNA using RCas9 and RFP fused to the Ras GTPase-activating protein-binding protein 1 (G3BP1) protein, a well-described marker for stress granules (Tourrière et al., 2003). Application of sodium arsenite to induce cellular stress results in an accumulation of mRNAs, including *ACTB* mRNA, into G3BP1-positive granules. We observed accumulation of RCas9 signal to G3BP1-positive foci in the presence of the RCas9 system targeting *ACTB* mRNA. To verify that this accretion of RCas9 signal required specific RNA recognition, we utilized three different sgRNAs and PAMmers targeting sequences from λ bacteriophage (NTC1–3; Figures 3A and 3B). Indeed, in these negative controls, increased signal in G3BP1-positive foci was not observed. We also evaluated the ability of RCas9 to track less-abundant transcripts *CCNA2* and *TFRC* mRNA to stress granules. Notably, we observed statistically significantly higher fractions of stress granules that accumulate RCas9 signal (39% and 23%, respectively) compared to non-targeting controls (Figures 3A and 3C). Next, we tracked RCas9 signal in stressed, live cells over time (Figure 3B). We observed accumulation of RCas9 signal in G3BP1-positive foci in a manner dependent on the presence of sgRNA- and PAMmer-targeting *ACTB* mRNA. We also observed that the rate and degree of RCas9 signal accumulation in stress granules is dependent on dosage of the stressor sodium arsenite (Figure 3D). These results indicate the potential of RCas9 as a means to generate time-resolved RNA localization measurements.

DISCUSSION

Effective RNA recognition by Cas9 in living cells while avoiding perturbation of the target transcript relies on careful design of the PAMmer and delivery of Cas9 and its cognate guide RNA to the appropriate cellular compartments. Binding of Cas9 to nucleic acids requires two critical features: a PAM DNA sequence and an adjacent spacer sequence antisense to the Cas9-associated sgRNA. By separating the PAM and sgRNA target among two molecules (the PAMmer oligonucleotide and the target mRNA) that only associate in the presence of a target mRNA, RCas9 allows recognition of RNA while avoiding the encoding DNA. To avoid unwanted degradation of the target RNA, the PAMmer is composed of a mixed 2′OMe RNA and DNA that does not form a substrate for RNase H. Further, the sgRNA features a modified scaffold that removes partial transcription termination sequences and a modified structure that promotes association with Cas9 (Chen et al., 2013). Other CRISPR/Cas systems have demonstrated RNA binding in bacteria (Hale et al., 2009; Sampson et al., 2013) or eukaryotes (Price et al., 2015), although these systems cannot discriminate RNA from DNA targets, feature RNA-targeting rules that remain unclear, or rely on large protein complexes that may be difficult to reconstitute in mammalian cells.

In this work, we demonstrate RCas9-based recognition of *GAPDH*, *ACTB*, *CCNA2*, and *TFRC* mRNAs in live cells. Because the U6-driven sgRNA is largely restricted to the nucleus, the NLS-tagged dCas9 allows association with its sgRNA and subsequent interaction with the target mRNA before nuclear co-export with the target mRNA. As an initial experiment, we evaluated the potential of RNA recognition with Cas9 by targeting *GAPDH* mRNA and evaluating degree of nuclear export of dCas9-mCherry (Figure 1B). Robust cytoplasmic localization of dCas9-mCherry in the presence of a sgRNA-targeting *GAPDH* mRNA compared to nuclear retention in the presence of a non-targeting sgRNA indicated that Cas9 association with the mRNA was sufficiently stable to support co-export from the nucleus.

RCas9 as an RNA-imaging reagent requires that RNA recognition by RCas9 does not interfere with normal RNA metabolism. Here, we show that RCas9 binding within the 3′ UTR of *Renilla* luciferase does not affect its mRNA abundance and translation (Figures 1F and 1G). The utility of RCas9 for imaging and other applications hinges on the recognition of endogenous transcripts, so we evaluated the influence of RCas9 targeting on *GAPDH* and *ACTB* mRNAs and observed no significant differences among the mRNA and protein abundances by western blot analysis and qRT-PCR (Figure S1). These results indicate that RCas9 targeting these 3′ UTRs does not perturb the levels of mRNA or encoded protein.

We also evaluated the ability of RCas9 to reveal RNA localization by comparing RCas9 signal patterns to FISH. We utilized a FISH probe set composed of tens of singly labeled probes targeting *ACTB* mRNA and compared FISH signal distributions to a single dCas9-GFP/sgRNA/PAMmer that recognizes the *ACTB* mRNA. Our findings indicate that the sgRNA primarily determines the degree of overlap among the FISH and RCas9 signals whereas the PAMmer plays a significant but secondary role. Importantly, in contrast to other untagged RNA localization determination methods such as FISH and molecular beacons, RCas9 is compatible with tracking untagged RNA localization in living cells and can be delivered rapidly to cells using established transfection methods. We also note that the distribution of *ACTB* mRNA was visualized using a single EGFP tag per transcript, and higher-sensitivity RNA tracking or single endogenous RNA molecule visualization may be possible in the future with RCas9 targeting multiple sites in a transcript or with a multiply tagged dCas9 protein.

Stress granules are translationally silent mRNA and protein accumulations that form in response to cellular stress and are increasingly thought to be involved with neurodegeneration (Li et al., 2013b). There are limited means that can track the movement of endogenous RNA to these structures in live cells (Bertrand et al., 1998). In addition to *ACTB* mRNA, we demonstrate that RCas9 is capable of measuring association of *CCNA2* and *TFRC* mRNA trafficking to stress granules (Figure 3A). Upon stress induction with sodium arsenite, we observed that 50%, 39%, and 23% of stress granules featured overlapping RCas9 foci when targeting *ACTB*, *TFRC*, and *CCNA2* mRNAs, respectively (Figure 3C). This result correlates with the expression levels of these transcripts (Figure S3) as *ACTB* is expressed about 8 and 11 times more highly than *CCNA2* and *TFRC*, respectively. We also observed that RCas9 is capable of tracking RNA localization over time as *ACTB* mRNA is trafficked to stress granules over a period of 30 min (Figure 3B). We noted a dependence of RCas9 signal accumulation in stress granules on stressor concentration (Figure 3D). This approach for live-cell RNA tracking stands in contrast to molecular beacons and aptamer-based RNA-tracking

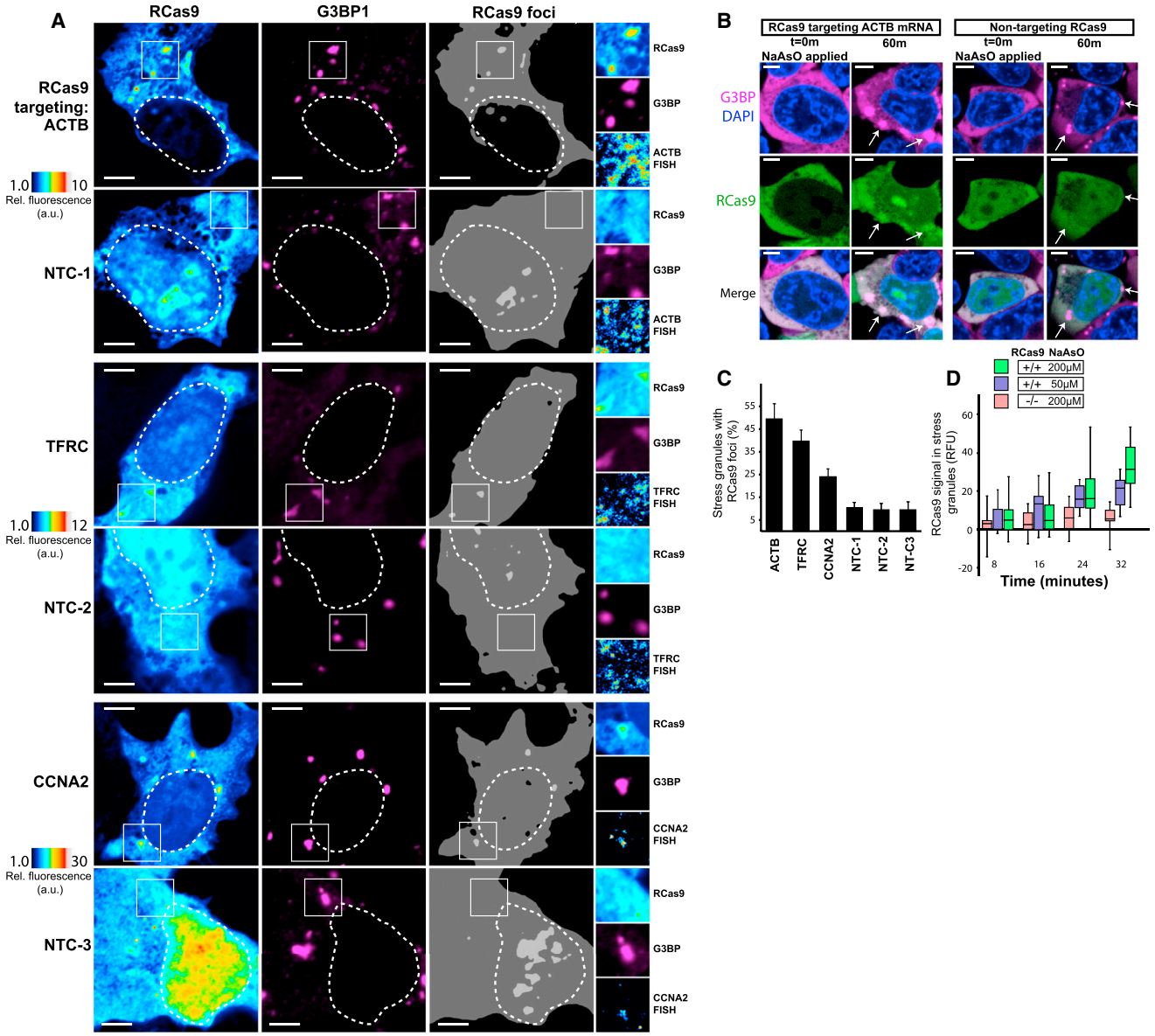

Figure 3. Tracking of mRNA Trafficking to Stress Granules with RCas9

(A) The RCas9 system targeting *ACTB*, *TFRC*, or *CCNA2* mRNAs or one of three non-targeting controls (NTCs) was delivered to HEK293T cells expressing G3BP1, a protein known to be trafficked to stress granules, fused to RFP. Cells were treated with sodium arsenite; fixed; subjected to FISH for *ACTB*, *TFRC*, or *CCNA2* mRNA; and imaged.

(B) RNA trafficking to stress granules was imaged in real time using cells harboring RCas9-targeting *ACTB* mRNA. At time zero, cells were imaged and sodium arsenite applied. Sixty minutes later, cells were imaged again, and a comparison of RCas9 and G3BP1-positive stress granules revealed close correlation of foci only in the presence of sgRNA- and PAMmer-targeting *ACTB* mRNA.

(C) The fraction of stress granules with RCas9 foci when targeting three mRNAs (*ACTB*, *TFRC*, and *CCNA2*) compared to three non-targeting controls. Error bars ± SD calculated from 50 cells from each of three biological replicates. p values among the RCas9 system targeting *ACTB*, *TFRC*, and *CCNA2* mRNA are <0.001 when compared to each of the NTC conditions. p values were calculated with Student's t test.

(D) In a similar experiment, RCas9-targeting *ACTB* mRNA signal accumulation in stress granules was tracked over time. Eight to eleven stress granules were tracked in each condition with time points every 8 min for 32 min.

Scale bars represent 5 microns. See also Figure S3.

methods, which suffer from delivery issues and/or require alteration of the target RNA sequence via incorporation of RNA tags.

Future applications of RCas9 could allow the measurement or alteration of RNA splicing via recruitment of split fluorescent proteins or splicing factors adjacent to alternatively spliced exons. Further, the nucleic-acid-programmable nature of RCas9 lends itself to multiplexed targeting (Cong et al., 2013) and the use of Cas9 proteins that bind orthogonal sgRNAs

(Esvelt et al., 2013) could support distinct activities on multiple target RNAs simultaneously. It is possible that the simple RNA targeting afforded by RCas9 could support the development of sensors that recognize specific healthy or disease-related gene expression patterns and reprogram cell behavior via alteration of gene expression or concatenation of enzymes on a target RNA (Delebecque et al., 2011; Sachdeva et al., 2014). Efforts toward Cas9 delivery in vivo are underway (Dow et al., 2015; Swiech et al., 2015; Zuris et al., 2015), and these efforts combined with existing oligonucleotide chemistries (Bennett and Swayze, 2010) could support in vivo delivery of the RCas9 system for targeted modulation of many features of RNA processing in living organisms.

RNA is subject to processing steps that include alternative splicing, nuclear export, subcellular transport, and base or backbone modifications that work in concert to regulate gene expression. The development of a programmable means of RNA recognition in order to measure and manipulate these processes has been sought after in biotechnology for decades. This work is, to our knowledge, the first demonstration of nucleic-acid-programmed RNA recognition in living cells with CRISPR/Cas9. By relying upon a sgRNA and PAMmer to determine target specificity, RCas9 supports versatile and unambiguous RNA recognition analogous to DNA recognition afforded by CRISPR/Cas9. The diverse applications supported by DNA-targeted CRISPR/Cas9 range from directed cleavage, imaging, transcription modulation, and targeted methylation, indicating the utility of both the native nucleolytic activity of Cas9 as well as the range of activities supported by Cas9-fused effectors. In addition to providing a flexible means to track this RNA in live cells, future developments of RCas9 could include effectors that modulate a variety of RNA-processing steps with applications in synthetic biology and disease modeling or treatment.

EXPERIMENTAL PROCEDURES

Plasmid Construction, PAMmer Synthesis, and Target Site Choice

The dCas9-2xNLS sequence was amplified from pHR-SFFV-dCas9-BFP-KRAB (a gift from Stanley Qi and Jonathan Weissman; Addgene plasmid no. 46911), tagged with two SV40 NLSs on the C terminus, and fused to EGFP or mCherry in pCDNA 3.1 (Life Technologies) using Gibson assembly. To construct the sgRNA scaffold construct, the human U6 polymerase III promoter with the modified sgRNA scaffold (Chen et al., 2013) was purchased as a gBlock from IDT with two *BbsI* restriction sites at the 5′ end of the sgRNA scaffold (see sequence in Table S2) and cloned into the multiple cloning site of pBlueScript II SK (+) (Agilent) using Gibson assembly. Phosphorylated oligonucleotides encoding the sgRNA sequences (with overhangs 5′CACC on the RNA antisense strand and 5′AAAC on the sense strand) were ligated into *BbsI*-digested sgRNA scaffold construct to produce sgRNAs targeting the 3′ UTR of *GAPDH*, *ACTB*, and *Renilla* luciferase mRNAs (see Tables S1 and S2). The luciferase-PEST construct for pull-down and abundance experiments was modified from plasmid pRLuc (gift from Jens Lykke-Andersen, UCSD). pCMV-*Renilla* luciferase is a version of the same construct lacking MS2 and RCas9 target sites.

RCas9 target sites were chosen with a combination of the IDT antisense oligonucleotide design tool and the microarray probe design tools Picky (Chou et al., 2004) and OligoWiz (Wernersson and Nielsen, 2005). We designed PAMmers against high-confidence sites with eight bases on the 5′ end beyond the PAM sequence. PAMmers were composed of mixed 2′OMe RNA and DNA bases and purified by HPLC (Integrated DNA Technologies).

Cell Lines

U2OS and HEK293T cells were grown in DMEM supplemented with 10% fetal bovine serum, Glutamax, penicillin/streptomycin, and non-essential amino acids (Life Technologies). Cells were passaged every 3 or 4 days with TrypLE EXPRESS (Life Technologies) using standard methods and maintained in a humidified incubator at 37°C with 5% CO_2.

GAPDH and ACTB mRNA Targeting with RCas9

U2OS cells cultured as described above were passaged at ~80% confluency. Glass-bottom 96-well plates or chamber slides were coated with 20 μg/ml fibronectin in PBS for 2 hr at 37°C and then the fibronectin solution was aspirated and 20,000 cells were plated in each well. Sixteen hours later, cells were transfected with the sgRNA and dCas9-2xNLS-EGFP plasmids using Lipofectamine 3000 (Life Technologies) according to the manufacturer's instructions. pCMV-*Renilla* luciferase was co-transfected in these experiments so that total transfected protein load was the similar among various dosages of sgRNA and dCas9. The mass ratio of sgRNA and dCas9-EGFP plasmids was 5:1 in experiments described in this work where the amount of dCas9-EGFP was fixed at 10% of total transfected material. Immediately after plasmid transfection, PAMmers were transfected using Lipofectamine RNAiMax (Life Technologies) according to manufacturer's instructions. Twenty-four hours after transfection, cells were washed with PBS and fixed with 3.7% paraformaldehyde in PBS, permeabilized with 70% ethanol at 4°C for 1 hr, and mounted using Prolong Gold Antifade mounting medium with DAPI (Life Technologies). Confocal microscopy was conducted using a Zeiss LSM 810 confocal microscope.

Nuclear export of RCas9 in the presence of sgRNA and PAMmer targeting the 3′ UTR of *GAPDH* mRNA was analyzed by measuring the average signal in the nuclei and cytoplasm of individual cells. Cells with average cytoplasmic signal greater than the average nuclear signal were considered positive and counted toward the fraction of cells with cytoplasmic RCas9 signal.

RNA Immunoprecipitation

HEK293T cells cultured as described above were passaged at 80% confluency, and 600,000 cells were seeded in each well of 6-well tissue culture plates coated with poly-*L*-lysine. Sixteen hours later, cells were co-transfected with the RCas9 system as described above or plasmids encoding MS2-EGFP or EGFP along with a plasmid encoding the model *Renilla* luciferase mRNA driven by a cytomegalovirus (CMV) promoter (Figure 1D). Twenty-four hours later, the growth media was aspirated and the cells were washed with PBS. 1% paraformaldehyde in PBS was applied to the cells, incubated for 10 min at room temperature, and then the solution was aspirated and the cells washed twice with cold PBS. Next, the cells were scraped from the wells in cold PBS and the cell suspension was centrifuged at 800 × *g* for 4 min to pellet the cells. The cells were washed once more and then resuspended in radioimmunoprecipitation assay (RIPA) buffer with protease inhibitors (Roche) and sonicated for 5 min in a Bioruptor sonicator (50% duty cycle; 1 min period). Insoluble material was pelleted after a high-speed centrifugation, and the supernatant was applied to protein G DynaBeads (Life Technologies) coated with mouse anti-GFP antibody (Roche). After overnight incubation at 4°C, the bead supernatant was retained and beads washed three times with RIPA buffer containing 0.02% Tween-20 and once with DNase buffer (350 mM Tris-HCl [pH 6.5]; 50 mM $MgCl_2$; 5 mM DTT). The beads were resuspended in DNase buffer and TURBO DNase (Life Technologies) was added to 0.08 units/μl. The beads were incubated at 37°C for 30 min, and then proteinase K (NEB) was added to 0.1 U/μl and incubated with shaking at 37°C for 30 min. Next, urea was added to 2.5 M and the beads were incubated with shaking at 37°C for 30 min. The bead supernatant was collected and subjected to two sequential phenol:chloroform:isoamyl alcohol (25:24:1) extractions followed by three chloroform extractions. The RNA was precipitated and reverse transcribed using SuperScript III (Life Technologies) using random hexamer primers, and relative abundance of *Renilla* luciferase RNA on the beads was compared to the supernatant using RT-PCR (see Table S3 for primer sequences).

Measurements of Influence of RCas9 on RNA Stability and Translation

HEK293T cells were cultured as described above, passaged and plated in 96- or 12-well tissue culture plates, and co-transfected 24 hr later with the

RCas9 system as described above and the *Renilla* luciferase construct carrying MS2 and RCas9 binding sites in the 3′ UTR. In the protein abundance measurements, a small amount of CMV-driven firefly luciferase vector (5% of total transfected plasmid) was co-transfected as a transfection control. For RNA stability measurements, RNA was isolated 24 hr after transfection, DNase treated, and reverse transcribed with Superscript III (Life Technologies) using dT(20) primers according the manufacturer's instructions. The amount of *Renilla* luciferase cDNA relative to *GAPDH* was then measured using RT-PCR (see Table S3 for primer sequences). For the translation studies, *Renilla* and firefly luciferase protein were measured with the Dual Luciferase Kit (Promega) according to the manufacturer's instructions.

For measuring the influence of RCas9 on *GAPDH* and *ACTB* mRNA and protein abundance, the RCas9 system targeting the 3′ UTR of each transcript, GFP alone, or RCas9 with the λ2-targeting sgRNA and PAMmer was transfected. Modified sgRNA vectors carrying pGK-driven blue fluorescent protein (BFP) were used in this experiment, and transfected cells were isolated using FACS gated on cells positive for GFP and BFP expression. Transfected cells were lysed and subjected to western blotting and RT-PCR for *ACTB*, *GAPDH*, and *TUBA1A* transcripts.

FISH

Stellaris FISH Probes recognizing human *ACTB*, *CCNA2*, and *TFRC* mRNAs and labeled with Quasar 670 (VSMF-2003-5; Biosearch Technologies) were hybridized to cells 24 hr after transfection with the RCas9 system. Hybridization was conducted according to the manufacturer's instructions. Confocal microscopy was conducted using an Olympus FV1000 confocal microscope or Zeiss LSM 810 confocal microscope.

Overlap Analysis for FISH and RCas9

Colocalization analysis among FISH and RCas9-targeting *ACTB* mRNA was conducted using the Coloc 2 plugin from the image analysis software FIJI (Schindelin et al., 2012). The cytoplasm of individual cells with similar dCas9-EGFP transfection levels was selected, and the Coloc 2 analysis was conducted using default parameters. The Manders' overlap coefficient describing degree of overlap of the FISH signal with RCas9 for more than 60 cells in each condition was compiled, and p values were calculated with the two-tailed Mann-Whitney U test.

Tracking ACTB mRNA Trafficking to Stress Granules

A HEK293T cell line was genetically modified with a fusion of RFP to the C terminus of Ras G3BP1 using CRISPR/Cas9. Briefly, a donor plasmid was constructed consisting of the RFP ORF, a puromycin selection cassette, and flanking 1.5-kb homology arms directed at the G3BP1 locus. An sgRNA sequence targeting the C terminus of G3BP1 was cloned into pSpCas9(BB)-2A-GFP (pX458) (gift from Feng Zhang; Addgene plasmid no. 48138) and co-transfected with the donor plasmid using Fugene HD (Roche) following the manufacturer's instructions. Forty-eight hours after transfection, cells were selected with 1 μg/ml puromycin in growth medium for 14 days and RFP-positive clones were selected and screened by PCR.

A clone with at least one modified allele was plated on glass chamber slides coated with fibronectin and transfected with the RCas9 system targeting the 3′ UTR of *ACTB*, *CCNA2*, or *TFRC* mRNA or one of three non-targeting sgRNA and PAMmer combinations (λ2–λ4) as described above (see Table S2 for sgRNA and PAMmer sequences). Twenty-four hours after transfection, cells were subjected to 200 μM sodium arsenite for 30 min, fixed, and subjected to FISH and imaged with a Zeiss LSM 810 confocal microscope. In a separate experiment, cells were stressed with varying concentrations of sodium arsenite and imaged with a Zeiss LSM 810 confocal microscope with a stage incubator over 32 min. Cells were maintained at 37°C in a humidified atmosphere and 5% CO_2 and imaged every 8 min.

Analysis of ACTB mRNA Trafficking to Stress Granules

Stress granules with average RCas9 signal at least 2-fold greater than surrounding cytoplasm were determined to be positive for RCas9. The average RCas9 signal in stress granules was calculated using the "measure" function in Fiji and compared to the average cytoplasmic RCas9 signal in the surrounding cytoplasm. RCas9-positive foci were visualized by dividing the value of each pixel by the average cytoplasmic signal, which reduced cytoplasmic signal to a value of "1" and RCas9-positive foci to a value of "2" or more. Next, a Gaussian blur was applied to improve foci definition. These images are reported in Figure 3A. The accumulation of RCas9 signal over time in stress granules was calculated by recording average signal intensity in the RCas9 channel in areas with overlapping G3BP1-RFP foci at each time point. Average signal intensity in the RCas9 channel surrounding G3BP1-RFP foci was recorded as background and subtracted from the previous value to produce the background-adjusted RCas9 signal in stress granules.

SUPPLEMENTAL INFORMATION

Supplemental Information includes three figures and three tables and can be found with this article online at http://dx.doi.org/10.1016/j.cell.2016.02.054.

AUTHOR CONTRIBUTIONS

Conceptualization, D.A.N., M.R.O., J.A.D., and G.W.Y.; Methodology, D.A.N. and M.R.O.; Investigation, D.A.N., M.Y.F., J.L.X., and S.J.M.; Writing – Original Draft, D.A.N. and G.W.Y.; Writing – Review & Editing, D.A.N., G.W.Y., and M.R.O.; Funding Acquisition, G.W.Y.; Supervision, G.W.Y.

ACKNOWLEDGMENTS

We acknowledge members of the G.W.Y. lab, particularly Ashleigh Schaffer, Stefan Aigner, and Ron Batra for critical comments. This work was supported by grants from the NIH (HG004659 and NS075449) and from the California Institute of Regenerative Medicine (RB3-05009 and RB4-06045) to G.W.Y. D.A.N. is supported by the National Science Foundation Graduate Research Fellowship (DGE-1144086) and Powell-Focht graduate fellowship. M.R.O. is supported by a CJ Martin fellowship from the National Health and Medical Research Council (Australia). J.A.D. is a Howard Hughes Medical Institute Investigator. G.W.Y. is an Alfred P. Sloan Research Fellow. J.A.D. is a co-founder of Editas Medicine, Intellia Therapeutics, and Caribou Biosciences and a scientific advisor to Caribou, Intellia, eFFECTOR Therapeutics, and Driver.

Received: November 15, 2015
Revised: February 5, 2016
Accepted: February 24, 2016
Published: March 17, 2016

REFERENCES

Bennett, C.F., and Swayze, E.E. (2010). RNA targeting therapeutics: molecular mechanisms of antisense oligonucleotides as a therapeutic platform. Annu. Rev. Pharmacol. Toxicol. *50*, 259–293.

Bertrand, E., Chartrand, P., Schaefer, M., Shenoy, S.M., Singer, R.H., and Long, R.M. (1998). Localization of ASH1 mRNA particles in living yeast. Mol. Cell *2*, 437–445.

Chen, B., Gilbert, L.A., Cimini, B.A., Schnitzbauer, J., Zhang, W., Li, G.W., Park, J., Blackburn, E.H., Weissman, J.S., Qi, L.S., and Huang, B. (2013). Dynamic imaging of genomic loci in living human cells by an optimized CRISPR/Cas system. Cell *155*, 1479–1491.

Chou, H.H., Hsia, A.P., Mooney, D.L., and Schnable, P.S. (2004). Picky: oligo microarray design for large genomes. Bioinformatics *20*, 2893–2902.

Cong, L., Ran, F.A., Cox, D., Lin, S., Barretto, R., Habib, N., Hsu, P.D., Wu, X., Jiang, W., Marraffini, L.A., and Zhang, F. (2013). Multiplex genome engineering using CRISPR/Cas systems. Science *339*, 819–823.

Delebecque, C.J., Lindner, A.B., Silver, P.A., and Aldaye, F.A. (2011). Organization of intracellular reactions with rationally designed RNA assemblies. Science *333*, 470–474.

Dow, L.E., Fisher, J., O'Rourke, K.P., Muley, A., Kastenhuber, E.R., Livshits, G., Tschaharganeh, D.F., Socci, N.D., and Lowe, S.W. (2015). Inducible in vivo genome editing with CRISPR-Cas9. Nat. Biotechnol. *33*, 390–394.

Please cite this article in press as: Nelles et al., Programmable RNA Tracking in Live Cells with CRISPR/Cas9, Cell (2016), http://dx.doi.org/10.1016/j.cell.2016.02.054

Esvelt, K.M., Mali, P., Braff, J.L., Moosburner, M., Yaung, S.J., and Church, G.M. (2013). Orthogonal Cas9 proteins for RNA-guided gene regulation and editing. Nat. Methods *10*, 1116–1121.

Filipovska, A., Razif, M.F., Nygård, K.K., and Rackham, O. (2011). A universal code for RNA recognition by PUF proteins. Nat. Chem. Biol. *7*, 425–427.

Fouts, D.E., True, H.L., and Celander, D.W. (1997). Functional recognition of fragmented operator sites by R17/MS2 coat protein, a translational repressor. Nucleic Acids Res. *25*, 4464–4473.

Hale, C.R., Zhao, P., Olson, S., Duff, M.O., Graveley, B.R., Wells, L., Terns, R.M., and Terns, M.P. (2009). RNA-guided RNA cleavage by a CRISPR RNA-Cas protein complex. Cell *139*, 945–956.

Hwang, W.Y., Fu, Y., Reyon, D., Maeder, M.L., Tsai, S.Q., Sander, J.D., Peterson, R.T., Yeh, J.R., and Joung, J.K. (2013). Efficient genome editing in zebrafish using a CRISPR-Cas system. Nat. Biotechnol. *31*, 227–229.

Li, D., Qiu, Z., Shao, Y., Chen, Y., Guan, Y., Liu, M., Li, Y., Gao, N., Wang, L., Lu, X., et al. (2013a). Heritable gene targeting in the mouse and rat using a CRISPR-Cas system. Nat. Biotechnol. *31*, 681–683.

Li, Y.R., King, O.D., Shorter, J., and Gitler, A.D. (2013b). Stress granules as crucibles of ALS pathogenesis. J. Cell Biol. *201*, 361–372.

Mali, P., Yang, L., Esvelt, K.M., Aach, J., Guell, M., DiCarlo, J.E., Norville, J.E., and Church, G.M. (2013). RNA-guided human genome engineering via Cas9. Science *339*, 823–826.

Manders, E.M., Stap, J., Brakenhoff, G.J., van Driel, R., and Aten, J.A. (1992). Dynamics of three-dimensional replication patterns during the S-phase, analysed by double labelling of DNA and confocal microscopy. J. Cell Sci. *103*, 857–862.

Nakayama, T., Fish, M.B., Fisher, M., Oomen-Hajagos, J., Thomsen, G.H., and Grainger, R.M. (2013). Simple and efficient CRISPR/Cas9-mediated targeted mutagenesis in Xenopus tropicalis. Genesis *51*, 835–843.

O'Connell, M.R., Oakes, B.L., Sternberg, S.H., East-Seletsky, A., Kaplan, M., and Doudna, J.A. (2014). Programmable RNA recognition and cleavage by CRISPR/Cas9. Nature *516*, 263–266.

Ozawa, T., Natori, Y., Sato, M., and Umezawa, Y. (2007). Imaging dynamics of endogenous mitochondrial RNA in single living cells. Nat. Methods *4*, 413–419.

Price, A.A., Sampson, T.R., Ratner, H.K., Grakoui, A., and Weiss, D.S. (2015). Cas9-mediated targeting of viral RNA in eukaryotic cells. Proc. Natl. Acad. Sci. USA *112*, 6164–6169.

Qi, L.S., Larson, M.H., Gilbert, L.A., Doudna, J.A., Weissman, J.S., Arkin, A.P., and Lim, W.A. (2013). Repurposing CRISPR as an RNA-guided platform for sequence-specific control of gene expression. Cell *152*, 1173–1183.

Sachdeva, G., Garg, A., Godding, D., Way, J.C., and Silver, P.A. (2014). In vivo co-localization of enzymes on RNA scaffolds increases metabolic production in a geometrically dependent manner. Nucleic Acids Res. *42*, 9493–9503.

Sampson, T.R., Saroj, S.D., Llewellyn, A.C., Tzeng, Y.L., and Weiss, D.S. (2013). A CRISPR/Cas system mediates bacterial innate immune evasion and virulence. Nature *497*, 254–257.

Sander, J.D., and Joung, J.K. (2014). CRISPR-Cas systems for editing, regulating and targeting genomes. Nat. Biotechnol. *32*, 347–355.

Schindelin, J., Arganda-Carreras, I., Frise, E., Kaynig, V., Longair, M., Pietzsch, T., Preibisch, S., Rueden, C., Saalfeld, S., Schmid, B., et al. (2012). Fiji: an open-source platform for biological-image analysis. Nat. Methods *9*, 676–682.

Sokol, D.L., Zhang, X., Lu, P., and Gewirtz, A.M. (1998). Real time detection of DNA.RNA hybridization in living cells. Proc. Natl. Acad. Sci. USA *95*, 11538–11543.

Sternberg, S.H., Redding, S., Jinek, M., Greene, E.C., and Doudna, J.A. (2014). DNA interrogation by the CRISPR RNA-guided endonuclease Cas9. Nature *507*, 62–67.

Swiech, L., Heidenreich, M., Banerjee, A., Habib, N., Li, Y., Trombetta, J., Sur, M., and Zhang, F. (2015). In vivo interrogation of gene function in the mammalian brain using CRISPR-Cas9. Nat. Biotechnol. *33*, 102–106.

Tourrière, H., Chebli, K., Zekri, L., Courselaud, B., Blanchard, J.M., Bertrand, E., and Tazi, J. (2003). The RasGAP-associated endoribonuclease G3BP assembles stress granules. J. Cell Biol. *160*, 823–831.

Unsworth, H., Raguz, S., Edwards, H.J., Higgins, C.F., and Yagüe, E. (2010). mRNA escape from stress granule sequestration is dictated by localization to the endoplasmic reticulum. FASEB J. *24*, 3370–3380.

Urnov, F.D., Rebar, E.J., Holmes, M.C., Zhang, H.S., and Gregory, P.D. (2010). Genome editing with engineered zinc finger nucleases. Nat. Rev. Genet. *11*, 636–646.

Wang, Y., Cheong, C.G., Hall, T.M., and Wang, Z. (2009). Engineering splicing factors with designed specificities. Nat. Methods *6*, 825–830.

Wernersson, R., and Nielsen, H.B. (2005). OligoWiz 2.0–integrating sequence feature annotation into the design of microarray probes. Nucleic Acids Res. *33*, W611–W615.

Wiedenheft, B., Sternberg, S.H., and Doudna, J.A. (2012). RNA-guided genetic silencing systems in bacteria and archaea. Nature *482*, 331–338.

Yang, D., Xu, J., Zhu, T., Fan, J., Lai, L., Zhang, J., and Chen, Y.E. (2014). Effective gene targeting in rabbits using RNA-guided Cas9 nucleases. J. Mol. Cell Biol. *6*, 97–99.

Zuris, J.A., Thompson, D.B., Shu, Y., Guilinger, J.P., Bessen, J.L., Hu, J.H., Maeder, M.L., Joung, J.K., Chen, Z.Y., and Liu, D.R. (2015). Cationic lipid-mediated delivery of proteins enables efficient protein-based genome editing in vitro and in vivo. Nat. Biotechnol. *33*, 73–80.

Cell

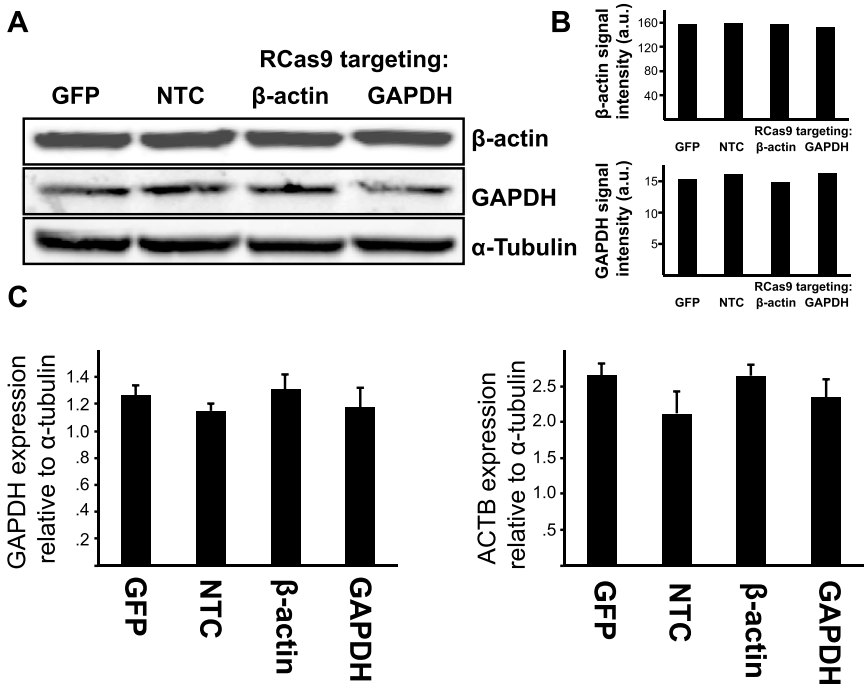

Figure S1. ACTB and GAPDH Protein and mRNA Levels in the Presence of RCas9 Targeting These mRNAs, Related to Figure 1

(A) The abundance of GAPDH and ACTB protein was measured by Western blot with TUBA1A as a loading control. Controls include non-targeting RCas9 labeled "NTC" (sgRNA and PAMmer targeting the λ2 sequence) and GFP transfected instead of the RCas9 system ("GFP").

(B) Quantification of the Western blot data.

(C) The abundance of *GAPDH* and *ACTB* mRNA was measured by RT-PCR relative to *TUBA1A*.

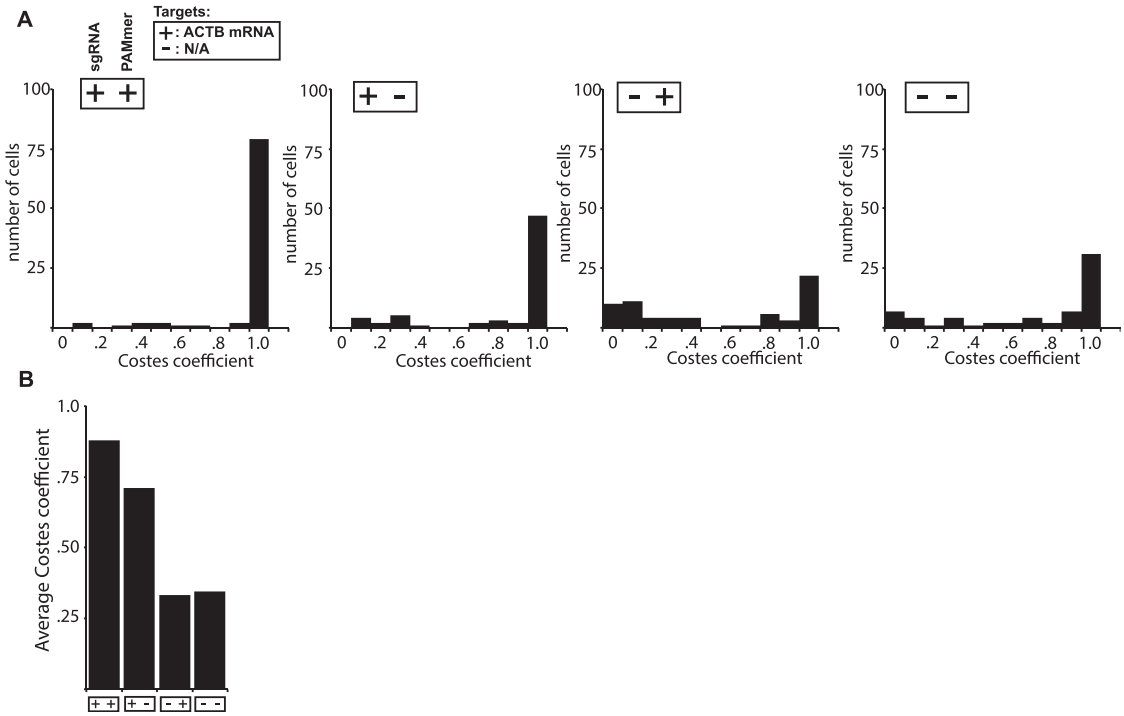

Figure S2. A Comparison of the Costes Coefficients from Individual Cells Measured in the Colocalization Analysis Conducted in Figure 2B

A Costes coefficient > 0.95 indicates that colocalization is unlikely due to random chance. See also Figure 2.

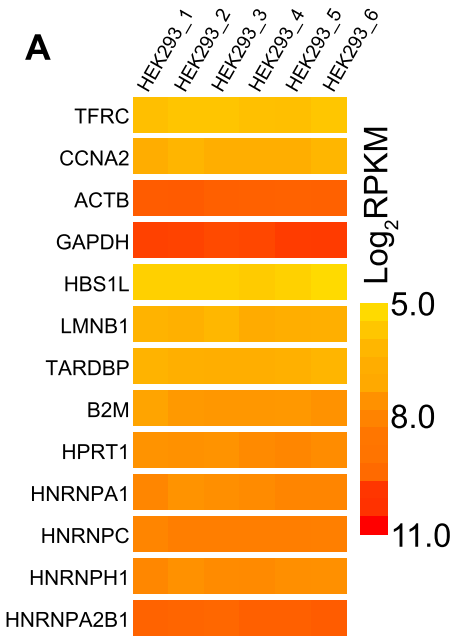

Figure S3. Expression Levels of the mRNAs Targeted in this Study Compared to Housekeeping Genes, Related to Figure 3
RNA-seq from six biological replicates was compared in terms of the reads per kilobase of transcript per million mapped reads (RPKM).

Cell, Volume *165*

Supplemental Information

Programmable RNA Tracking in Live Cells with CRISPR/Cas9

David A. Nelles, Mark Y. Fang, Mitchell R. O'Connell, Jia L. Xu, Sebastian J. Markmiller, Jennifer A. Doudna, and Gene W. Yeo

Supplemental Table 1. RNA target sequences, related to Figures 1-3.

Target	PAMmer target underlined, sgRNA target **bold**
GAPDH mRNA 3'UTR	CACAAGAGGAAGAGAGAGA**CCCUCACUGCUGGGGAGUCC**
β-actin mRNA 3'UTR	GAAGGUGACAGCAGUCGGU**UGGAGCGAGCAUCCCCCAAA**
Cyclin A2 mRNA 3'UTR	CUGACAUUCAUUUUCCUAA**GCAACUGGAUCAAUUUGCUG**
Transferrin receptor 3'UTR	AGGGGUUGCUAAGAAGCGA**GCACUGACCAGAUAAGAAUG**
λ2	GCUCAAUUUUGACAGCGGU**CAUGGCAUUCCACUUAUCAC**
λ3	GGAAAUCAUUCAACACCCG**CACUAUCGGAAGUUCACCAG**
λ4	GCAAUAAAAAUGCGCGCCU**GAACCACCAGGCUAUAUCUG**

Supplemental Table 2. PAMmer and sgRNA sequences, related to Figures 1-3. The PAM and spacer sequences are listed in bold.

PAMmer, β-actin 3'UTR	mUCmGCmUCmCA**mUGG**mGAmCTmGCmUGmUCmACmCTmUC
sgRNA, β-actin 3'UTR	**GUUUGGGGGAUGCUCGCUCCA**GUUUAAGAGCUAUGCUGGA AACAGCAUAGCAAGUUUAAAUAAGGCUAGUCCGUUAUCAA CUUGAAAAAGUGGCACCGAGUCGGUGCUUUUUUU
PAMmer, GAPDH 3'UTR	mAGmUGmAGmGG**mCGG**mCTmCTmCTmUCmCTmCTmUGmUG
sgRNA, GAPDH 3'UTR	**GGACUCCCCAGCAGUGAGGG**GUUUAAGAGCUAUGCUGGAA ACAGCAUAGCAAGUUUAAAUAAGGCUAGUCCGUUAUCAAC UUGAAAAAGUGGCACCGAGUCGGUGCUUUUUUU
PAMmer, λ2 (NTC-1)	mATmGCmCAmUGm**UGG**mGCmUGmUCmAAmAAmUTmGAmGC
sgRNA, λ2 (NTC-1)	**GUGAUAAGUGGAAUGCCAUG**GUUUAAGAGCUAUGCUGGAA ACAGCAUAGCAAGUUUAAAUAAGGCUAGUCCGUUAUCAAC UUGAAAAAGUGGCACCGAGUCGGUGCUUUUUUU
PAMmer, λ3 (NTC-2)	mCGmATmAGmUGm**CGG**mGTmGTmUGmAAmUGmATmUTmCC
sgRNA, λ3 (NTC-2)	**GCUGGUGAACUUCCGAUAGUG**GUUUAAGAGCUAUGCUGGA AACAGCAUAGCAAGUUUAAAUAAGGCUAGUCCGUUAUCAA CUUGAAAAAGUGGCACCGAGUCGGUGCUUUUUUU
PAMmer, λ4 (NTC-3)	mGGmUGmGTmUCm**UGG**mCGmCGmCAmUTmUTmUAmUTmGC
sgRNA, λ4 (NTC-3)	**GCAGAUAUAGCCUGGUGGUUC**GUUUAAGAGCUAUGCUGGA AACAGCAUAGCAAGUUUAAAUAAGGCUAGUCCGUUAUCAA CUUGAAAAAGUGGCACCGAGUCGGUGCUUUUUUU
PAMmer, cyclin A2 3'UTR	mCCmAGmUTmGCmU**GG**mGGmAAmAAmUGmAAmUGmUCmAG
sgRNA, cyclin A2 3'UTR	**GCAGCAAAUUGAUCCAGUUGC**GUUUAAGAGCUAUGCUGGA AACAGCAUAGCAAGUUUAAAUAAGGCUAGUCCGUUAUCAA CUUGAAAAAGUGGCACCGAGUCGGUGCUUUUUUU
PAMmer, transferrin receptor 3'UTR	mGTmCAmGTmGCmU**GG**mCTmUCmUTmAGmCAmACmCCmCT
sgRNA, transferrin receptor 3'UTR	**GCAUUCUUAUCUGGUCAGUGC**GUUUAAGAGCUAUGCUGGA AACAGCAUAGCAAGUUUAAAUAAGGCUAGUCCGUUAUCAA CUUGAAAAAGUGGCACCGAGUCGGUGCUUUUUUU
U6 promoter-2xBbsi-sgRNA scaffold	**TGTACAAAAAAGCAGGCTTTAAAGGAACCAATTCAGTCGA CTGGATCCGGTACCAAGGTCGGGCAGGAAGAGGGCCTATT TCCCATGATTCCTTCATATTTGCATATACGATACAAGGCT GTTAGAGAGATAATTAGAATTAATTTGACTGTAAACACAA AGATATTAGTACAAAATACGTGACGTAGAAAGTAATAATT TCTTGGGTAGTTTGCAGTTTTAAAATTATGTTTTAAAATG GACTATCATATGCTTACCGTAACTTGAAAGTATTTCGATT TCTTGGCTTTATATATCTTGTGGAAAGGACGAAACACC**GG GTCTTCGAGAAGACCTGTTTAAGAGCTATGCTGGAAACAG CATAGCAAGTTTAAATAAGGCTAGTCCGTTATCAACTTGA AAAAGTGGCACCGAGTCGGTGCTTTTTTT

Supplemental Table 3: qPCR primer sequences, related to Figures 1 and S1

GAPDH forward primer	AAGGTGAAGGTCGGAGTCAAC
GAPDH reverse primer	GGGGTCATTGATGGCAACAATA
Renilla luciferase forward primer	GTAACGCTGCCTCCAGCTAC
Renilla luciferase reverse primer	GTGGCCCACAAAGATGATTT
β-tubulin forward primer	AAGATCCGAGAAGAATACCCTGA
β-tubulin reverse primer	CTACCAACTGATGGACGGAGA
ACTB forward primer	CATGTACGTTGCTATCCAGGC
ACTB reverse primer	CTCCTTAATGTCACGCACGAT